European Journal of Mechanics / B Fluids 96 (2022) 1–14

Contents lists available at ScienceDirect

European Journal of Mechanics / B Fluids

journal homepage: www.elsevier.com/locate/ejmflu

# SPH numerical modelling of landslide movements as coupled two-phase flows with a new solution for the interaction term

Saeid Moussavi Tayyebi [a,*], Manuel Pastor [a], Miguel Martin Stickle [a], Ángel Yagüe [b], Diego Manzanal [b], Miguel Molinos [a], Pedro Navas [b]

[a] Department of Mathematics and Computers Applied to Civil and Naval Engineering, ETS Ingenieros de Caminos, Universidad Politécnica de Madrid, Calle del Profesor Aranguren, 3, 28040 Madrid, Spain

[b] Department of Continuum Mechanics and Theory of Structures, ETSI Caminos, Canales y Puertos, Universidad Politécnica de Madrid, Calle del Profesor Aranguren, 3, 28040 Madrid, Spain

ARTICLE INFO

*Article history:*
Available online 22 June 2022

*Keywords:*
Interaction force
Permeability
Depth integrated model
Couple problems
Two phases
SPH
Dam-break
Acheron rock avalanche

ABSTRACT

In this paper, the theoretical framework is a depth-integrated two-phase model capable of considering many essential physical aspects such as reproducing the propagation of debris flows with soil permeability ranging from high to low and considering the pore-water pressure evolution. In this model, the pore fluid is described by an additional set of depth-integrated balance equations in order to take into account the velocity of pore fluid. The model employs a frictional rheological law for the granular material, and the interstitial fluid is treated as a Newtonian fluid. A drag law describes the interaction between interstitial fluid and grains. The variables of permeability, porosity, and drag force are included in the governing equations to consider the interaction between the phases. This paper aims to extend a generalized two-phase depth-integrated model to enhance the description of the interaction between the two phases and their respective movements. It allows us to increase our understanding of the mechanism behind natural rapid landslides. To evaluate the developed approach, a set of dam-break problems has been performed. These simulations provide interesting information in simple and controlled situations on the landslide propagations with different degrees of soil permeability and the interaction between solid and fluid phases. The extended model has also been applied to simulate the dynamics of the Acheron rock avalanche, which is an appropriate benchmark to examine the applicability of the model to real cases.



## 1. Introduction

Every year thousands of landslide-related phenomena, including rock avalanches and debris flows, cause loss of human lives and destruction in their path. The analyses of this kind of natural hazard require the evaluation of stability of the source area as well as the prediction of propagation behaviour (runout distance, velocities, thickness, and shape of deposit). In this study, we deal with the latter issue by using reliable models for reproducing the dynamics of these flows. The main characteristics of fast landslide in the propagation stage are (i) coupling between phases due to mixtures of solid particles and pore fluids, (ii) the relative velocities between the solid and fluid phases, and (iii) development of pore-water pressures in excess to hydrostatic. Once the flow characteristics are predicted, we can develop more precise hazard maps and design more effective countermeasures.

Four kinds of mathematical models are commonly used to reproduce the dynamic behaviour of debris flow, including (i) one-phase propagation models, (ii) one-phase propagation-consolidation models, (iii) two-phase propagation models, and (iv) two-phase propagation–consolidation models.

*One-phase models*, represented by Bagnold [1], can be applied for limited cases where the soil is treated as a one-phase non-Newtonian material, such as granular flows where the soil permeability is high enough so that the consolidation time is much shorter than the time of propagation and the material behaves as drained. It is worth mentioning the pioneering paper on granular flows by Savage and Hutter [2,3].

In *one-phase propagation–consolidation models*, the flowing mass is still treated as a one-phase material. However, the role of pore pressure evolution is taken into account. These models have been applied by Iverson [4], Iverson and Denlinger [5] to debris flows, and by Pastor et al. [6,7] to flow slides and debris flows.

* Corresponding author.
*E-mail addresses:* saeid.moussavita@upm.es (S.M. Tayyebi), manuel.pastor@upm.es (M. Pastor), miguel.martins@upm.es (M.M. Stickle), angel.yague@upm.es (Á. Yagüe), d.manzanal@upm.es (D. Manzanal), m.molinos@alumnos.upm.es (M. Molinos), pedro.navas@upm.es (P. Navas).

https://doi.org/10.1016/j.euromechflu.2022.06.002

In *two-phase propagation models*, the effects of velocity difference between the phases are taken into account. But, the excess pore-water pressure evolution is neglected by assuming that the soil permeability is very large. Pitman and Le [8] and Pudasaini [9] used this kind of models in an Eulerian formulation, and Pastor et al. [10,11] used them in a Lagrangian formulation.

In *two-phase propagation–consolidation models*, it is assumed that the excess pore-water pressure persists throughout the entire solid skeleton of the debris flow and increases its mobility. General two-phase models considering pore-water pressures were proposed by Bui et al. [12] for 3D models and Pastor et al. [13] for depth-integrated models.

The existing mathematical models can basically be divided into one-phase and two-phase propagation–consolidation models to describe the complex dynamic behaviours of debris flows. One-phase models are less time-consuming, while the two-phase models produce more accurate results. However, two-phase models are computationally expensive due to employing drag laws to consider the interactions between the phases. This paper presents a new solution for the interaction term that significantly facilitates the computations of two-phase models.

This paper also evaluates the two-phase propagation-consolidation model developed by Pastor et al. [13] to illustrate its performance and reveal some important aspects of the model hidden in the previous papers. The model was developed to take into account essential physical aspects of fast landslides, including strong coupling between solid and fluid phases, pore-water pressure evolution, and porosity variations. Therefore, the developed two-phase propagation–consolidation model with a solution for the interaction term will be described and evaluated using several benchmark exercises.

Following this introductory section, we will present the generalized two-phase model used to simulate the mechanical behaviour of landslides. It consists of two linear momentum balance equations, two mass balance equations, which are completed using a consolidation equation, a frictional rheological model, and an interaction law. These depth-integrated mathematical equations are discretized using the Smoothed Particle Hydrodynamics Method (SPH) for the balance equations and the Finite Difference Method (FDM) for the consolidation equation. In this section, the two-phase model has also been extended to achieve a precise and effective methodology to replicate the complex behaviour of fast landslides by including an essential physical phenomenon of velocities evolution based on drag forces.

Next, to provide some insight into the basic features of the presented governing equations, the developed two-phase model is applied to 1D dam-break problems, which provide interesting information in simple and controlled situations. The influences of interaction forces and porosity variations are considered in the simulations. The propagation of debris flows with different soil permeability is analysed by using different models. Then, the effects of drag force, porosity variation, and pore-water pressure evolution on the dynamic behaviours of each phase are discussed. The numerical results demonstrate new features of the extended model. Finally, the applicability of the model is evaluated through back-analyzing of a natural rock avalanche, aiming to test the capability of the model to reproduce the complex behaviour of a real landslide.

## 2. Computational model

### 2.1. Mathematical model

In two-phase modelling, the interaction force's magnitude determines whether the solid and fluid phases separate from each other or remain mixed. The interaction between solid and fluid phases plays an important role in the dynamics of debris flows. Therefore, a two-phase model should be applied to capture the dynamic of each phase. In this paper, the two-phase propagation–consolidation model proposed by Pastor el at. [13] is applied. It is based on the depth-integrated mathematical model of Zienkiewicz and Shiomi [14]. The authors evaluated the capacity of the model to reproduce a debris flow on a laboratory-scale inclined channel [15] and a real terrain [16] by comparing the numerical results with the measurements obtained from experiments and the data obtained from in-depth field investigation, respectively. It is capable of reproducing the propagation of debris flows with different soil permeability ranging from high to low. The governing equations consist of 2D shallow-water equations including two balance equations of linear momentum and two balance equations of mass, expressed in Eulerian form, describing the solid and the fluid phases, and a consolidation equation describing the evolution of pore pressure along the vertical axis, as follows:

(i) Mass balance equations:

$$\frac{\bar{d}^{(s)}h_s}{dt} + \nabla\cdot(h_s\bar{\boldsymbol{v}}_s) = \bar{n}_s e_R \tag{1}$$

$$\frac{\bar{d}^{(w)}h_w}{dt} + \nabla\cdot(h_w\bar{\boldsymbol{v}}_w) = \bar{n}_w e_R \tag{2}$$

(ii) Linear momentum balance equations:

$$\begin{aligned}\rho_s h_s\frac{\bar{d}^{(s)}\bar{\boldsymbol{v}}_s}{dt} = {}& \rho_s\nabla\left(\frac{1}{2}b_3 h h_s + \frac{\Delta\bar{p}_w h\bar{n}}{\rho_s}\right)\\ & - \left(\frac{1}{2}\rho_w b_3 h^2 - \Delta\bar{p}_w h\right)\nabla\bar{n}_s\\ & + \boldsymbol{\tau}_B^{(s)} + \rho_s\boldsymbol{b}h_s + \bar{\boldsymbol{R}}h - \rho_s\bar{\boldsymbol{v}}_s\bar{n}_s e_R\end{aligned} \tag{3}$$

$$\begin{aligned}\rho_w h_w\frac{\bar{d}^{(w)}\bar{\boldsymbol{v}}_w}{dt} = {}& \rho_w\nabla\left(\frac{1}{2}b_3 h h_w - \frac{\Delta\bar{p}_w h\bar{n}}{\rho_w}\right)\\ & - \left(\frac{1}{2}\rho_w b_3 h^2 - \Delta\bar{p}_w h\right)\nabla\bar{n}_w\\ & + \boldsymbol{\tau}_B^{(w)} + \rho_w\boldsymbol{b}h_w - \bar{\boldsymbol{R}}h - \rho_w\bar{\boldsymbol{v}}_w\bar{n}_w e_R\end{aligned} \tag{4}$$

where the internal forces consist of pressure terms, $\bar{P}_s = b_3 h h_s/2 + \Delta\bar{p}_w h\bar{n}/\rho_s$ and $\bar{P}_w = b_3 h h_w/2 + \Delta\bar{p}_w h\bar{n}/\rho_w$ acting on solid or fluid phases respectively, and a porosity gradient term. $\Delta\bar{p}_w$ is the excess pore-water pressure. An overbar over a magnitude denotes a depth-integrated value. We denote some parameters by the sub-indexes s for solid and w for fluid phases. External forces consist of basal shear stress ($\boldsymbol{\tau}_B$), gravity force ($b_3 = -g$), and interaction force ($\bar{R}$). $e_R$ is an erosion coefficient. As can be seen in Eqs. (3) and (4), in two-phase models, each phase is characterized by its density ($\rho$), averaged velocity ($\bar{\boldsymbol{v}}$), height ($h$), and averaged porosity ($\bar{n}$). $\boldsymbol{b}$ is the vector of body forces.

(iii) Consolidation equation: The interaction between solid and the pore fluid is considerably stronger for flowing mass consisting of low-permeability soil. Debris flow height and porosity variations also have a considerable effect on excess pore-water pressure evolution. Therefore, pore pressure description is the key to modelling such phenomena. In depth-integrated models, the vertical structure of the magnitudes is lost, as the only available information is their depth-integrated values. This is why simple one-phase models cannot describe pore pressure evolution along with depth. It is, therefore, necessary to implement additional

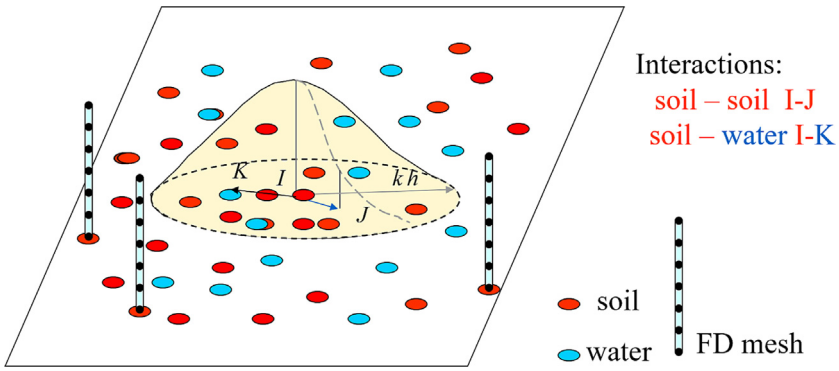


**Fig. 1.** SPH integration in the particle support for two-phase: (1) soil–soil (I-J) and (2) soil–water (I-K) with a 1D finite-difference mesh at each SPH node that represents a solid particle.

equations describing how pore pressure evolves along time and depth.

$$\frac{d^{(s)}\Delta p_w}{dt} = -\rho_d' b_3 \frac{d^{(s)}h}{dt} + c_v \frac{\partial^2 \Delta p_w}{\partial {x_3}^2} - E_m \frac{1}{(1-\bar{n})}\frac{d^{(s)}\bar{n}}{dt} \quad (5)$$

which describes pore pressure evolution and consists of three terms, including (i) debris flow height variations, (ii) consolidation along vertical axis, (iii) depth-averaged porosity variations, respectively. $c_v$ is a consolidation coefficient obtained by multiplying permeability ($k_w$) by volumetric stiffness ($k_v$). $\rho_d'$ is the effective density and $E_m$ ($= 3k_v\,(1-2\nu)$) oedometric modulus. $\nu$ is the Poisson's ratio.

The interested reader will find in the article by Pastor et al. [13] interesting descriptions of these mathematical equations. The consolidation time can be obtained by using the parameters of consolidation coefficient and saturated height ($h_{\text{sat}}$) as [17]:

$$t_c = \frac{4h_{\text{sat}}^2}{\pi^2 c_v} \quad (6)$$

### 2.2. Numerical methods

The partial differential equations of the previous section should be discretized and transformed to a form suitable for particle-based simulation. In the simulation model developed by Pastor et al. [13], the balance of mass and momentum equations have been discretized with the meshless numerical method of Smoothed particle hydrodynamics (SPH), while the consolidation equation has been discretized using a set of finite difference meshes. Therefore, two sets of nodes are introduced, one to represent the solid particles' movement and another to represent the fluid particles' movement, and a 1D finite-difference mesh for describing the pore-water pressure (pwp) along the vertical axis, as depicted in Fig. 1. The meshless numerical method of SPH, invented by Lucy [18] and Gingold and Monaghan [19] to model astrophysical problems, has been successfully applied in the area of Solid Mechanics [20,21] and particularly in the modelling of debris flows [22–24] and fast landslides [25,26]. Concerning depth-integrated SPH models for landslide propagation, it is worth mentioning Pastor et al. (2009a) [27], McDougall and Hungr [28], Rodríguez Paz and Bonet [29], and Goodwin and Choi [30]. Good reviews can be found in the texts of Liu and Liu or Li and Liu [31,32]. GIS-based SPH numerical models have also been used for simulating the kinematics of landslides over complex terrain [33,34]. Regarding water-related natural landslides using SPH models, it is worth mentioning Manenti et al. [35,36].

The results are a set of ordinary differential equations produced in discretized form with respect to time, as follows:

(i) Height re-initialization:

$$h_{ai} = \sum_j M_{aj} W_{ij} \quad (7)$$

where subscript $a$ denotes the solid ($s$) or fluid ($w$) phase. $M$ is a fictitious volume and $W$ smoothing kernel function. The interested reader can find interesting descriptions of these parameters in the article by Pastor et al. [37]. Subscripts $i$ and $j$ in the above equation denote particles $i$ and $j$ as shown in Fig. 1.

(ii) Linear momentum balance equation:

$$\begin{aligned}\frac{\bar{d}^{(a)}\bar{\boldsymbol{v}}_{ai}}{dt} = &-\sum_{j=1}^{Nh} m_{aj}\left(\frac{\bar{P}_{ai}}{h_{ai}^2} + \frac{\bar{P}_{aj}}{h_{aj}^2}\right)\nabla W_{ij} \\ &- \left(\frac{1}{2}\frac{\rho_w}{\rho_a} b_3 h_i^2 - \frac{\Delta\bar{p}_w h_i}{\rho_a}\right)\sum_{j=1}^{Nh} m_{aj}\left(\frac{\bar{n}_{ai}}{h_{ai}^2} + \frac{\bar{n}_{aj}}{h_{aj}^2}\right)\nabla W_{ij} \\ &+ \frac{1}{\rho_a h_{ai}}\boldsymbol{\tau}_B^{(a)} + \boldsymbol{b}_i + \frac{1}{\rho_a}\bar{\boldsymbol{R}}_a - \frac{1}{h_{ai}}\bar{\boldsymbol{v}}_{ai}\bar{n}_{ai}e_R\end{aligned} \quad (8)$$

(iii) Consolidation equation, which is more suitable for the formulation of FDM:

$$\begin{aligned}\frac{d^{(s)}\Delta p_w}{dt} = &-\rho_d' b_3 \frac{d^{(s)}h}{dt}\left(1 - \frac{x_3}{h}\right) + c_v \frac{\partial^2 \Delta p_w}{\partial {x_3}^2} \\ &- E_m \frac{1}{(1-\bar{n})}\frac{d^{(s)}\bar{n}}{dt}\end{aligned} \quad (9)$$

As an alternative, the basal excess pore-water pressure can be approximated by solving the second term of Eq. (9) with the Fourier series using a quarter cosines shape function, with a zero value at the surface and zero gradients at the basal surface and assuming that there exists no porosity variation at the basal surface—the third term of Eq. (9) is eliminated. Thus, the time-evolution of excess pore-water pressure at the basal surface is given by:

$$\frac{d^{(s)}\Delta p_w^b}{dt} = -\rho_d' b_3 \frac{dh}{dt} - \beta \Delta p_w^b \quad (10)$$

where for simplification, we introduce $\beta$ as:

$$\beta = \frac{c_v \pi^2}{4h^2} = \frac{1}{t_c} \quad (11)$$

The resulting ordinary differential equations are discretized in time with the 4th order Runge Kutta method [38] in the SPH and the FTCS (Forward Time Centered Space) method in the FDM. The presented model is capable of taking into account the evolution

of excess pore-water pressure along the vertical axis in a depth-integrated model. This model, developed by Pastor et al. [13], can be applied to reproduce the complex dynamics behaviour of fast landslides containing low permeability soil with strong excess pore-water pressure. Next, the model will be generalized using a novel velocity-drag expression for cases with high permeability soil and large relative velocity between the solid and fluid phases.

### 2.3. Rheological and constitutive laws

The governing equations presented in the previous section have to be complemented by suitable rheological and constitutive equations. We need to provide the following items: (i) basal shear stress ($\boldsymbol{\tau_B}$), (ii) interaction force ($\bar{\boldsymbol{R}}$) and an (iii) erosion coefficient ($e_R$).

The basal shear stress ($\boldsymbol{\tau_B}$) is computed through Voellmy's friction law [39] modified to account for the effect of excess pore pressure at the basal surface. The basal shear stress is given by:

$$\boldsymbol{\tau_B} = \left(\rho_d^{'} g h - \Delta p_w^b\right) \frac{\bar{\boldsymbol{v}}_{\boldsymbol{i}}}{|\bar{\boldsymbol{v}}|} \tan\phi_B + \rho g \frac{|\bar{\boldsymbol{v}}|}{\xi} \bar{\boldsymbol{v}}_i \tag{12}$$

where $h$ is the propagation height, $\phi_B$ the basal friction angle, $\bar{\boldsymbol{v}}$ the depth-averaged flow velocity, $\xi$ the turbulence coefficient, and $\Delta p_w^b$ the excess pore-water pressure at the basal surface which is computed by using consolidation Eq. (10).

To couple the two sets of conservation equations, the interaction forces are defined to cover the contributions of both solid and fluid phases in the mixture. The interaction between two constituents is described by a term implemented in the linear momentum balance equations. It plays an important role in modelling two-phase debris flows as its effects on the dynamic behaviour of both solid and fluid phases are significant. Here, we introduce $\bar{\boldsymbol{R}}_s$ as the internal force on the solid particles due to the relative velocity of the fluid phase, and $\bar{\boldsymbol{R}}_w$ as the force on the fluid phase caused by the solid particles. Then, the following relation can be written:

$$\bar{\boldsymbol{R}} = \bar{\boldsymbol{R}}^{(s)} = (1-\bar{n})\,\bar{\boldsymbol{R}}_s = -\bar{\boldsymbol{R}}^{(w)} = -\bar{n}\bar{\boldsymbol{R}}_w \tag{13}$$

A wide range of drag force expressions can be found in the literature [40–43]. These expressions are capable of describing the interaction between grains and pore fluid in two-phase models. They control porosities, velocities, and the relative movement between the solid and fluid phases.

The Darcy law is a simple interaction model which has a linear relationship with the relative velocity. In this law, the interaction force is given by:

$$\bar{\boldsymbol{R}} = C_d\,(\bar{\boldsymbol{v}}_w - \bar{\boldsymbol{v}}_s) \tag{14}$$

where $C_d$ is the drag coefficient and plays an important role in the dynamics of debris flow propagation. It determines the forces needed to avoid the relative movement between the phases, and consequently, reduce the relative velocity between them. A large value of $C_d$ is equivalent to assume that a big drag force is applied from the granular phase to the fluid phase of the mixture, which produces less relative movement and separation.

In this paper, the interaction force between the two phases is modelled through the Anderson and Jackson law [40]. This law was used by Pitman and Le [8] for cases with large relative velocity. It is given by:

$$\bar{\boldsymbol{R}} = \frac{\bar{n}\,(1-\bar{n})}{V_T \bar{n}^m}\,(\rho_s - \rho_w)\,g\,(\bar{\boldsymbol{v}}_w - \bar{\boldsymbol{v}}_s) \tag{15}$$

in which the interaction force $\bar{\boldsymbol{R}}$ depends on the terminal velocity ($V_T$). $m$ is related to the Reynold number of the flow (1 for linear and 2 for quadratic).

As can be seen in Eq. (8), the phase velocities are related through an interaction term:

$$\frac{d^{(s)}\bar{\boldsymbol{v}}_s}{dt} = \cdots + \frac{1}{(1-\bar{n})\,\rho_s}\bar{\boldsymbol{R}} \tag{16}$$

$$\frac{d^{(w)}\bar{\boldsymbol{v}}_w}{dt} = \cdots - \frac{1}{\bar{n}\rho_w}\bar{\boldsymbol{R}} \tag{17}$$

Considering Eq. (14), the above equation can be rewritten as:

$$\frac{d^{(s)}\bar{\boldsymbol{v}}_s}{dt} = \cdots + \frac{1}{(1-\bar{n})\,\rho_s} C_d\,(\bar{\boldsymbol{v}}_w - \bar{\boldsymbol{v}}_s) \tag{18}$$

$$\frac{d^{(w)}\bar{\boldsymbol{v}}_w}{dt} = \cdots - \frac{1}{\bar{n}\rho_w} C_d\,(\bar{\boldsymbol{v}}_w - \bar{\boldsymbol{v}}_s) \tag{19}$$

Introducing $C_s = C_d/(1-n)\,\rho_s$, $C_w = C_d/n\rho_w$, and $\alpha = C_s/C_w$, the above equations can be rewritten as:

$$\frac{d}{dt}\begin{pmatrix}\bar{\boldsymbol{v}}_s\\ \bar{\boldsymbol{v}}_w\end{pmatrix} = \cdots + C_w \begin{pmatrix}-\alpha & \alpha\\ 1 & -1\end{pmatrix}\begin{pmatrix}\bar{\boldsymbol{v}}_s\\ \bar{\boldsymbol{v}}_w\end{pmatrix} \tag{20}$$

The above first-order linear differential equation is solved with the eigenvalue method, and the following solution for velocity–drag expression can be obtained:

$$\bar{\boldsymbol{v}}_s = \frac{1}{1+\alpha}\left[(\bar{\boldsymbol{v}}_{s0} + \alpha\bar{\boldsymbol{v}}_{w0}) + \alpha\,(\bar{\boldsymbol{v}}_{s0} - \bar{\boldsymbol{v}}_{w0})\exp\left(-C_w\,(1+\alpha)\,\Delta t\right)\right] \tag{21}$$

$$\bar{\boldsymbol{v}}_w = \frac{1}{1+\alpha}\left[(\bar{\boldsymbol{v}}_{s0} + \alpha\bar{\boldsymbol{v}}_{w0}) - (\bar{\boldsymbol{v}}_{s0} - \bar{\boldsymbol{v}}_{w0})\exp\left(-C_w\,(1+\alpha)\,\Delta t\right)\right] \tag{22}$$

where, considering Eq. (8), $\bar{\boldsymbol{v}}_{s0}$ and $\bar{\boldsymbol{v}}_{w0}$ can be obtained as follows:

$$\begin{aligned}\frac{\bar{d}^{(\alpha)}\bar{\boldsymbol{v}}_{\boldsymbol{s0i}}}{dt} = &-\sum_{j=1}^{Nh} m_{sj}\left(\frac{\bar{P}_{si}}{h_{si}^2} + \frac{\bar{P}_{sj}}{h_{sj}^2}\right)\nabla W_{ij}\\ &-\left(\frac{1}{2}\frac{\rho_w}{\rho_s}b_3 h_i^2 - \frac{\Delta\bar{p}_w h_i}{\rho_s}\right)\sum_{j=1}^{Nh} m_{sj}\left(\frac{\bar{n}_{si}}{h_{si}^2} + \frac{\bar{n}_{sj}}{h_{sj}^2}\right)\nabla W_{ij}\\ &+\frac{1}{\rho_s h_{si}}\boldsymbol{\tau}_{\boldsymbol{B}}^{(\alpha)} + \boldsymbol{b}_i - \frac{1}{h_{si}}\bar{\boldsymbol{v}}_{\boldsymbol{s0i}}\bar{n}_{si}e_R\end{aligned} \tag{23}$$

$$\begin{aligned}\frac{\bar{d}^{(\alpha)}\bar{\boldsymbol{v}}_{\boldsymbol{w0i}}}{dt} = &-\sum_{j=1}^{Nh} m_{wj}\left(\frac{\bar{P}_{wi}}{h_{wi}^2} + \frac{\bar{P}_{wj}}{h_{wj}^2}\right)\nabla W_{ij}\\ &-\left(\frac{1}{2}b_3 h_i^2 - \frac{\Delta\bar{p}_w h_i}{\rho_w}\right)\sum_{j=1}^{Nh} m_{wj}\left(\frac{\bar{n}_{wi}}{h_{wi}^2} + \frac{\bar{n}_{wj}}{h_{wj}^2}\right)\nabla W_{ij}\\ &+\frac{1}{\rho_w h_{wi}}\boldsymbol{\tau}_{\boldsymbol{B}}^{(\alpha)} + \boldsymbol{b}_i - \frac{1}{h_{wi}}\bar{\boldsymbol{v}}_{\boldsymbol{w0i}}\bar{n}_{wi}e_R\end{aligned} \tag{24}$$

It is a simple solution for Eq. (20) and contributes to the expressions of depth-averaged linear momentum balance Eq. (8) associated with an interaction force term. The velocities evolution of solid and fluid phases can be computed by using the above equations. Fig. 2 shows the results of the velocity evolution in the case of medium-permeability soil ($V_T = 0.1$ m/s, $\bar{n} = 0$, $\rho_s = 2000$, $\rho_w = 1000$, and $m = 1$) by assuming that the initial velocities of solid and fluid phases are 0 m/s and 1 m/s, respectively.

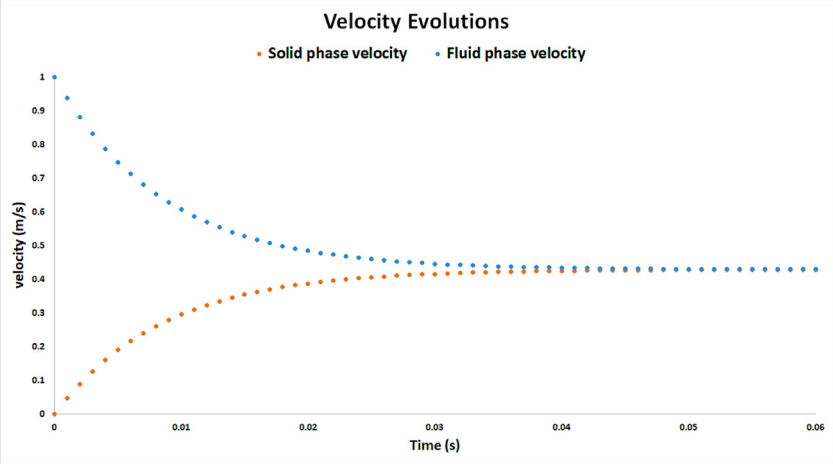


**Fig. 2.** Velocity evolution of solid and fluid phases with respect to time.

**Table 1**
The proposed velocity-drag expressions with their limits and conditions.

| | $n_L < n < 1 - n_L$ | $n \to 1$ | $n \to 0$ |
|---|---|---|---|
| $0 < C_w < \infty$ | Eqs. (21) and (22) | Eq. (25) | Not consistent |
| $C_w \to \infty$ | $\bar{v}_w = \bar{v}_s = \frac{\alpha}{1+\alpha}(\bar{v}_{s0} + \alpha \bar{v}_{w0})$ | $\bar{v}_s = \bar{v}_{w0}$<br>$\bar{v}_w = \bar{v}_{w0}$ | Eq. (26) |
| $C_w \to 0$ | $\bar{v}_s = \frac{1}{1+\alpha}[(\bar{v}_{s0} + \alpha \bar{v}_{w0}) + \alpha(\bar{v}_{s0} - \bar{v}_{w0})] = \bar{v}_{s0}$<br>$\bar{v}_w = \frac{1}{1+\alpha}[(\bar{v}_{s0} + \alpha \bar{v}_{w0}) - (\bar{v}_{s0} - \bar{v}_{w0})] = \bar{v}_{w0}$ | $\bar{v}_s = \bar{v}_{s0}$<br>$\bar{v}_w = \bar{v}_{w0}$ | Not consistent |

In the new velocity-drag expression given in Eqs. (21) and (22), the drag force plays an important role in the two-phase model and is capable of equilibrating the velocity difference between the phases, as shown in Fig. 2.

In some cases, the soil permeability is very high, and pore-fluid flows out the solid skeleton. In these cases, the proposed formulation of velocity evolution cannot be used after the porosity reaches a lower limit ($n_L$). Once we reached this point, the impact of drag forces on both phases should be different. To overcome these solid and fluid limit, we propose the following formulations:

(i) For fluid limit ($n \geq 1 - n_L$):

$$\begin{aligned} \bar{\boldsymbol{v}}_s &= \bar{\boldsymbol{v}}_{w0} + (\bar{\boldsymbol{v}}_{s0} - \bar{\boldsymbol{v}}_{w0}) \exp(-C_d \Delta t) \\ \bar{\boldsymbol{v}}_w &= \bar{\boldsymbol{v}}_{w0} \end{aligned} \tag{25}$$

(ii) For solid limit ($n \leq n_L$)

$$\begin{aligned} \bar{\boldsymbol{v}}_s &= \bar{\boldsymbol{v}}_{s0} \\ \bar{\boldsymbol{v}}_w &= \bar{\boldsymbol{v}}_{s0} \end{aligned} \tag{26}$$

(iii) For $n_L < n < 1 - n_L$: the general velocity-drag expressions given in Eqs. (21) and (22).

For convenience, we have provided the limits and conditions for the proposed expressions in Table 1.

The model presented in this work has been implemented in a code, using the programming language of Fortran, called "GeoFlow-SPH", developed at the Polytechnic University of Madrid by an expert research team for more than a decade. It has previously been applied to theoretical [44], experimental [15], and real case histories [45]. Many researchers [11,46,24,47] in different institutions have been using and validating the numerical code. In this study, all the proposed velocity-drag expressions with their conditions given in Table 1 have been implemented in the code.

The GeoFlow-SPH code contains various empirical erosion laws, including (i) Hungr erosion law [48], which is based on an algorithm that the total volume of debris increases in accordance with a specified rate, and (ii) Egashira erosion law [49], which is based on flume tests. The interested reader will find in the article by Pirulli and Pastor [50] interesting descriptions of these erosion laws. Pastor et al. [51] recently developed an arbitrary Lagrangian–Eulerian (ALE) model to consider pore-water pressure existing in the eroded materials.

Before starting the following section, it is important to note that a few realistic simplifying assumptions, which are acceptable for many engineering purposes, are considered in the model to obtain the approximate solutions. The fluidized soil will be assumed to consist of a solid skeleton and a fluid phase (two-phase), in which the fluid fills completely the voids (fully saturated: $S_r = 1$). In most cases, the fluid phase is inviscid and it is either water or a mixture of water with very fine soil particles such as clay, which can be considered a fluid. The porosity lower limit ($n_L$) is considered as 0.01. In this study, we use the variable smoothing length formula proposed by Benz [52], and the required properties of each point are determined using the cubic spline kernel [53]).

## 3. Case studies

### 3.1. Dam-break problems

1D dam-break exercises provide interesting information and some insight into developed models. They show the main aspects of the model in a simple and controlled situation [54,35]. We start by explaining how the results of the dam break problems will be represented to facilitate the interpretation. In depth-integrated models, the particles cannot be defined along the vertical axis. In these models, the flowing mass is divided into a finite number of columns represented by particles. To facilitate the visualization, two partial heights corresponding to the solid ($h_s$) and fluid

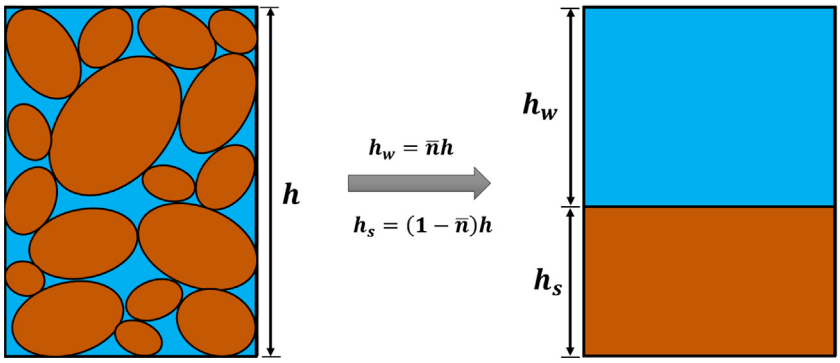


**Fig. 3.** Scheme for obtaining partial heights of both phases.

($h_w$) phases will be plotted in each model. The sum of these partial heights is the total height ($h$) of the mixture. As shown in Fig. 3, the phases are simulated in different layers. However, these phases interact with each other through a drag law that depends on the variables of porosity and permeability of the soil.

Let $n_w = n$ and $n_s = (1 - n)$ be the fraction of volume occupied by the water and solid particles, respectively. The heights of the solid phase ($h_s$) and fluid phase ($h_w$) are given by:

$$h_s = \bar{n}_s h \\ h_w = \bar{n}_w h \tag{27}$$

The initial conditions of the two-phase dam-break problem over a horizontal plane are presented in Fig. 3, where the initial heights of the debris flow are $h_s = 4$ m and $h_w = 6$ m, and the length is 10 m. The densities of solid and fluid particles are $\rho_s = 2000$ kg/m$^3$ and $\rho_w = 1000$ kg/m$^3$, respectively, an initial porosity ($\bar{n}_0$) of 0.6, for which the mixture density is $\rho = 1400$ kg/m$^3$. The 1D channel, with a length of 160 m, contains a dam situated at a distance of 10 m. The material is contained between a wall on the right side and a dam situated at the left side at the initial time. Once the dam is suddenly removed, the material liquefies, and the debris flow propagates along the horizontal plane.

It is important to note that in these simulations, it has been assumed that the granular soil has a basal frictional angle ($\phi$) of 45° and the turbulence coefficient ($\xi$) of 100 m/s$^2$. To obtain the interaction force ($\bar{\boldsymbol{R}}$), we applied Anderson drag law (see Eq. (15)) by assuming that the terminal velocity ($V_T$) be equal to 0.01 m/s, 0.1 m/s, and 3 m/s, corresponding to the cases having low, medium, and high-permeability soil, respectively, and $m = 1$. In these dam-break problems, the propagation time is approximately 13 s. Using Eq. (6), the consolidation times are obtained as 272 s, 27 s, and 0.04 s, corresponding to the cases having low, medium, and high-permeability soil, respectively. In these dam break problems, the SPH-FD model, using Eqs. (7)–(9), has been carried out to estimate the run-out distance and the deposition heights the debris flows during the propagation stage.

*First set of dam break problems*: When consolidation time is much shorter than propagation time, the pore pressures dissipate rapidly, and the material behaviour can be described as drained. As examples, we can mention granular flows, rock avalanches and debris flows consisting of soils with high permeability.

In Fig. 4, the curved lines result from the propagation modelling in which pore-water pressure is not considered. They coincide with the results of the models capable of considering pore-water pressure evolution (dashed lines). In these cases with high-permeability soil, it can be observed how the solid phase stops (brown curved and dashed line) while the water (blue curved and dashed line) continues flowing. As can be seen in Fig. 4, the excess pore-water pressure does not present any considerable influence on debris flow with high-permeability soil. In these cases, the excess pore-water pressure is not generated due to the high permeability of the soil and the flow's high velocity. The consolidation process does not occur during the propagation stage.

The one-phase models treat the soil as a dry granular material (black curved line and red dashed dot) due to the assumption that the fluid phase's acceleration is very small. Therefore, it is not a sufficient model for the cases of high-permeability soil. Still, it can be applied to landslides if the relative movement of water and solid can be neglected. On the other hand, two-phase models are capable of considering solid and fluid phases separately and take into account the difference of velocities in both phases.

Debris flows, particularly those consisting of high-permeability soil, can be analysed by two-phase models without needing to consider pore pressure. In this type of debris flows, an advantage of using two-phase models is their capability to simulate the fluid behaviour of the mixture when passing through the solid skeleton.

*Second set of dam break problems*: In this case, the time scale of pore-pressure dissipation is similar to the time scale of propagation. The intermediate case requires accurate modelling of pore pressure changes in the mixture. The pore-water pressure persisted during propagation until the debris flow reached the deposition area. Therefore, quantitative modelling of excess pore pressure time-space evolution is a fundamental issue to assess these cases. As shown in Fig. 5, a notable change of front evolution demonstrates the considerable effect of the excess pore-water pressure on the case with medium permeability. Besides, the solid and fluid phases of the mixture may have different velocities. Accordingly, two-phase modelling should be applied to consider the velocities of both solid and fluid phases and their mutual interaction.

*Third set of dam break problems*: If the consolidation time is much larger than the propagation time, the behaviour is described as "undrained", such as a flow of slurries with a high water content, where the dissipation time is much longer than the propagation time.

As shown in Fig. 6, interaction forces between phases play an important role in the two-phase case with low-permeable soil. The front propagation of the solid and fluid phases (brown curved line and blue dashed line, respectively) coincides.

The flows simulated by the two-phase model have longer travel distances compared to the one-phase cases due to the rheological parameters selected; otherwise, they will coincide with one another. In one-phase models, the results are more sensitive to the value of frictional angle. On the other hand, employing more input parameters in two-phase models always allows better matching between the simulation results and measurements. The

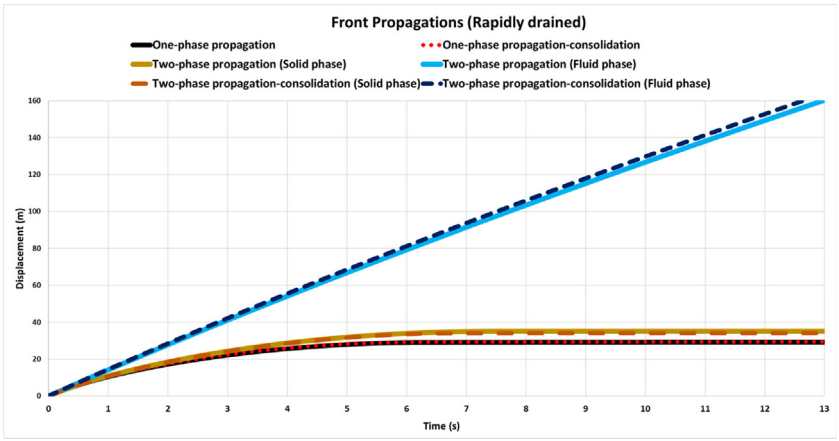


**Fig. 4.** Comparison of the front propagation of debris flows consisting of high-permeability soil obtained with different models. (For interpretation of the references to colour in this figure legend, the reader is referred to the web version of this article.)

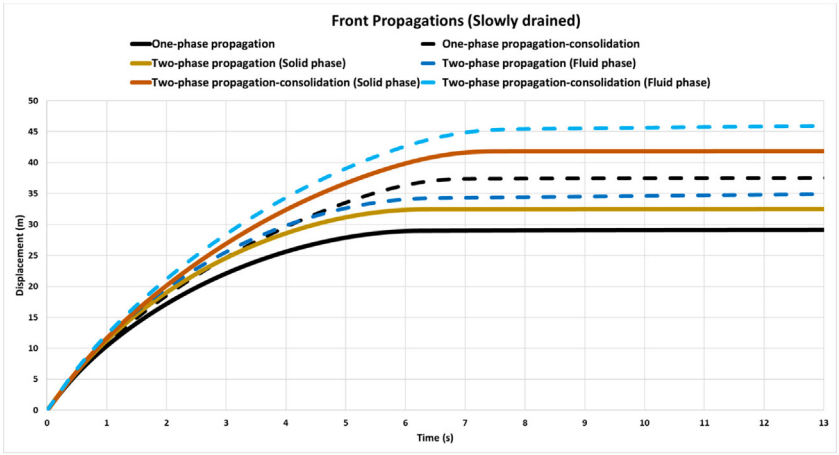


**Fig. 5.** Comparison of the front propagation of debris flows consisting of medium-permeability soil obtained with different models.

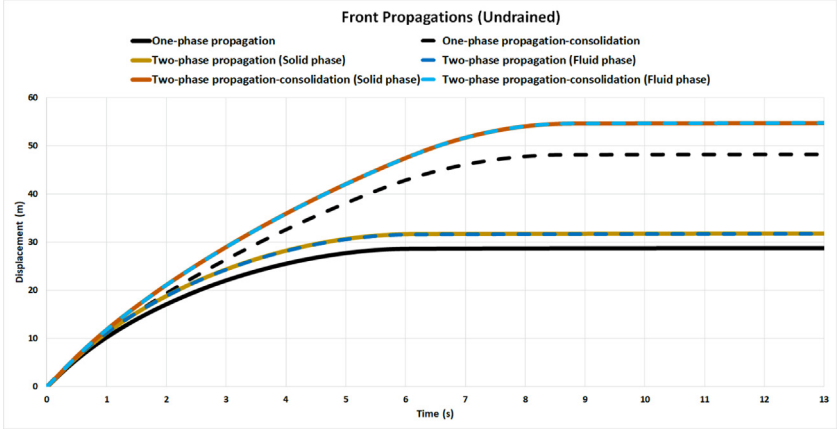


**Fig. 6.** Comparison of the front propagation of debris flows consisting of small-permeability soil obtained with different models.

interested reader will find in the article by Pastor et al. [37] interesting applications of the one-phase dam-break problem. Haddad et al. [44] and Pastor et al. [22] compared the results of the one-phase depth-integrated SPH model and an analytical solution [55,56] obtained from dam-break exercises.

We provide the profiles of total height and porosity at different time steps for three dam break problems with different soil permeability. As shown in Fig. 7-a, the initial porosities ($n_0$) of the mixtures are 0.6 and are evolving during the propagating stage. As depicted in Fig. 7, a large volume of fluid has abandoned the solid skeleton in the simulations with high permeability. Once the porosity value approaches unity, it indicates that the dominant phase is the fluid. In this stage, the porosity reaches the upper limit, and Eqs. (25) or (26) are deployed to compute the drag forces between the phases. The figure clearly shows the drag forces between phases are not strong enough to mobilize the

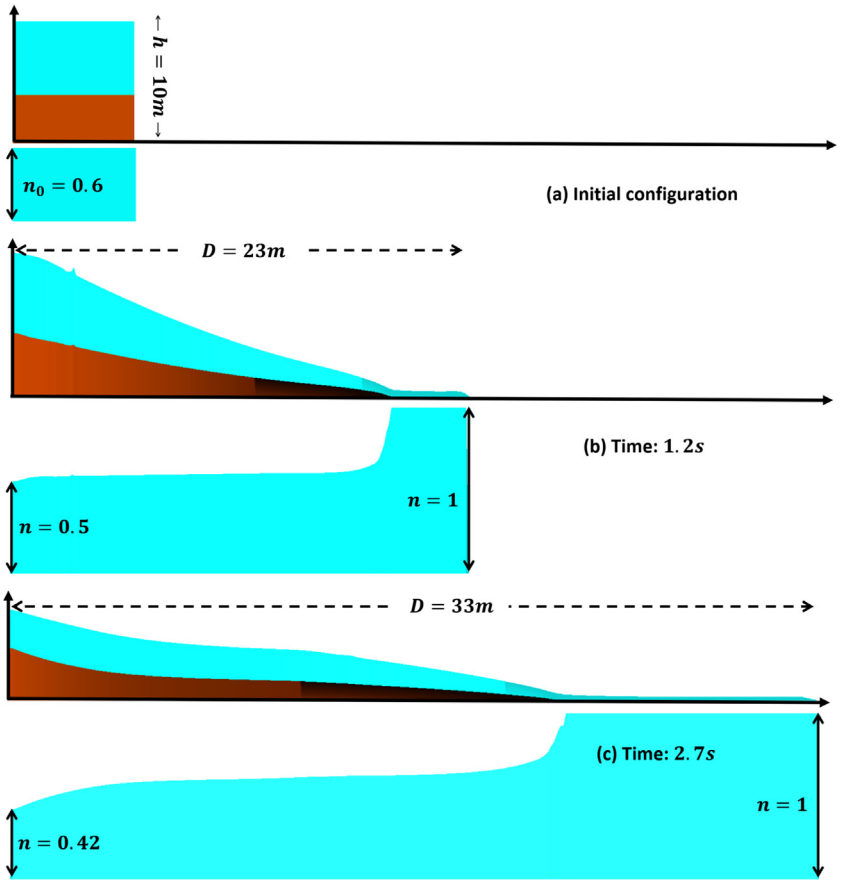


**Fig. 7.** (a) Initial configuration of the-dam break problems with the initial porosity profile. (b–c) Profiles of the propagation heights with their porosity profiles for the debris flows consisting of high-permeability soil at different time steps.

solid particles. Consequently, in these cases, porosity increases and reaches the value of 1 once water is abandoning the solid skeleton.

It is interesting to solve the same problem this time with a debris flow consisting of medium-permeability soil. Results of total heights together with the evolution of the porosity are shown in Fig. 8. In this case, the phases move relatively close to each other during the propagation, and a lower amount of fluid abandons the solid skeleton.

Finally, to complete the numerical simulations, the propagation heights, accompanied with their respective porosity profile, of the third scenario with low permeability have been depicted in Fig. 9. As shown in the figure, the velocities of both phases are very close to each other, and the porosity remains constant during propagation.

### 3.2. Acheron rock avalanche

In the previous papers, the two-phase model developed by Pastor et al. [13] was validated by simulating two real cases of the Sham Tseng San Tsue debris flow [13] and Yu Tung debris flow [16] occurred in Hong Kong in 1999 and 2008, respectively. This paper tests the two-phase model, incorporated with the proposed velocity-drag expression, by reproducing the propagation of a real case of rock avalanche that we have accessed to its reliable data.

The Acheron rock avalanche occurred in Canterbury, New Zealand, approximately 1100 years BP [57,58] based on radiocarbon dating analysis. An earthquake may have triggered the landslide as it is located close to fault zones. This example is based on the reliable information found in the package provided, which included (i) a digital terrain model, (ii) initial thickness and (iii) impacted area, showing the extension of the deposit. It is very important to note that the impacted area and deposition shape is one of the important characteristic of landslide in order to assess potential risks and design possible countermeasures. The extended model was applied to simulate the dynamics of the Acheron rock avalanche, which is an appropriate benchmark problem due to the availability of reliable information including topography, estimated deposition thickness and observed impact area, depicted in Fig. 10.

The Acheron Rock Avalanche was back-analyzed by Mergili et al. [59] using the r.avaflow code. The same geotechnical parameters are used here to simulate the rock avalanche with the extended model. The densities of solid and fluid particles have been taken as $\rho_s = 2700$ kg/m$^3$ and $\rho_w = 1000$ kg/m$^3$, respectively, and an initial porosity of 0.2, for which the mixture density is $\rho = 2350$ kg/m$^3$. The simulation model applies the Voellmy friction law (15) with a basal friction angle of 17°. Turbulence coefficient is disregarded in this particular case.

It is important to note that the numerical results of the developed model are more sensitive to the variables of terminal velocity ($V_T$), stiffness of the mixture ($k_v$), and consequently, the consolidation coefficient ($C_v$). Therefore, the characteristic times of propagation and consolidation are the key aspects of the proposed model. The numerical analysis was performed using a 1 m × 1 m Digital Terrain Model (DTM). The initial mass was schematized into two sets of 2100 SPH computational points, one representing solid particles and the other representing fluid particles, 1 m spaced.

In this real case study, no information has been provided about consolidation parameters mentioned in the previous

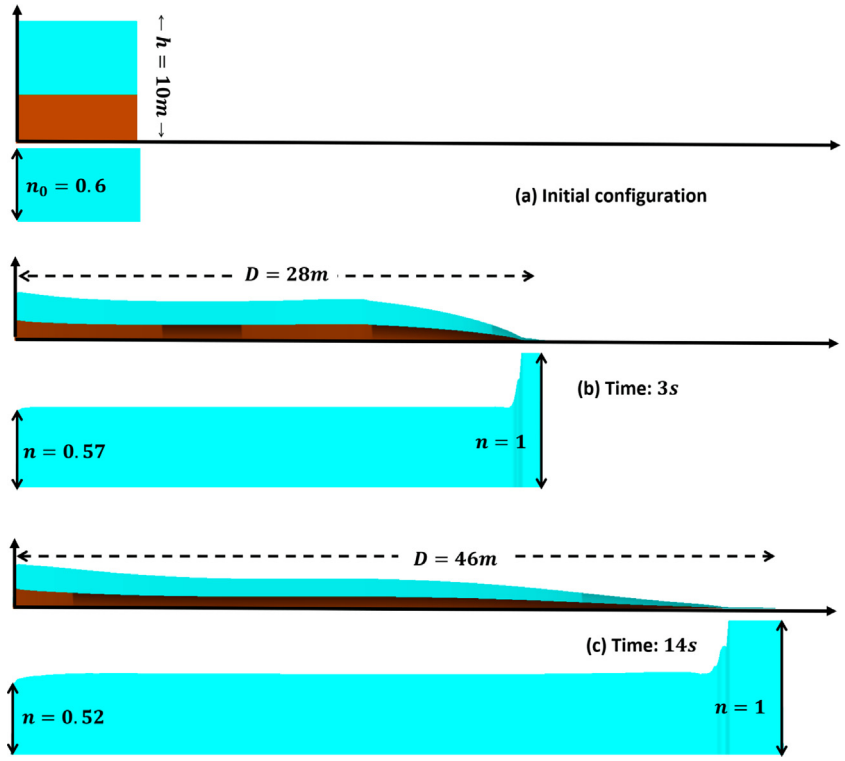


**Fig. 8.** (a) Initial configuration of the-dam break problems with the initial porosity profile. (b–c) Profiles of the propagation heights with their porosity profiles for the debris flows consisting of medium-permeability soil at different time steps.

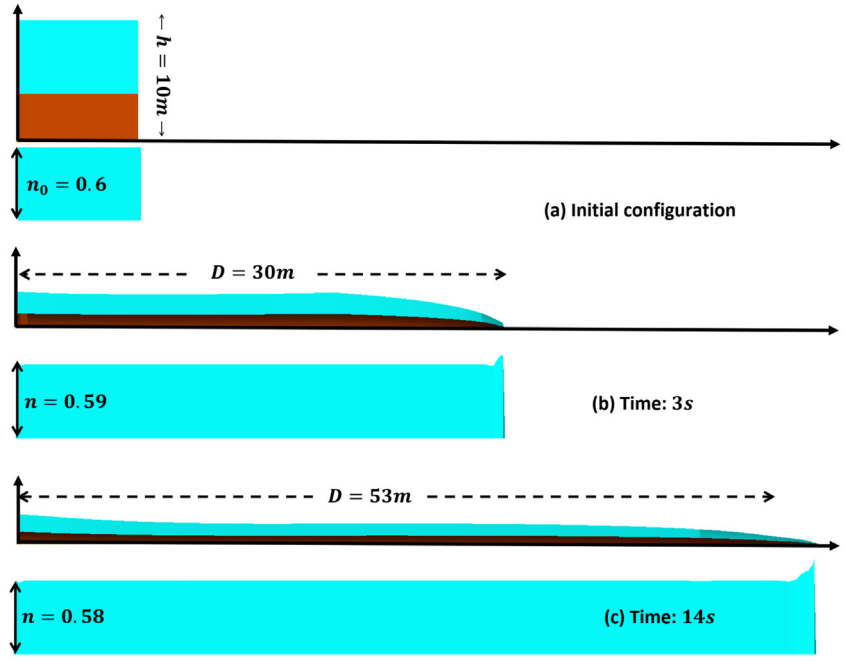


**Fig. 9.** (a) Initial configuration of the-dam break problems with the initial porosity profile. (b–c) Profiles of the propagation heights with their porosity profiles for the debris flows consisting of low-permeability soil at different time steps.

paragraph. Therefore, the modelers have to choose or back-calculate these values. In this model, consolidation Eq. (10) is applied to approximate the vertical distribution of excess pore-water pressure.

To back-analysis the debris avalanche, first, we assume that the flow consists of low-permeability soil. Regarding this scenario with low-permeability soil, we have chosen the values of $5 \times 10^{-4}$ m/s and $4 \times 10^{8}$ N/m$^2$ for the terminal velocity ($V_T$) and the mixture stiffness ($k_v$), respectively. In Fig. 11, we provide a topographical map showing the rock avalanche path and positions of the mass flow produced by the developed model at two different time steps. The trimline, which delineates the impacted area, based on the provided information [57,58] has also shown in Fig. 11-a:d.

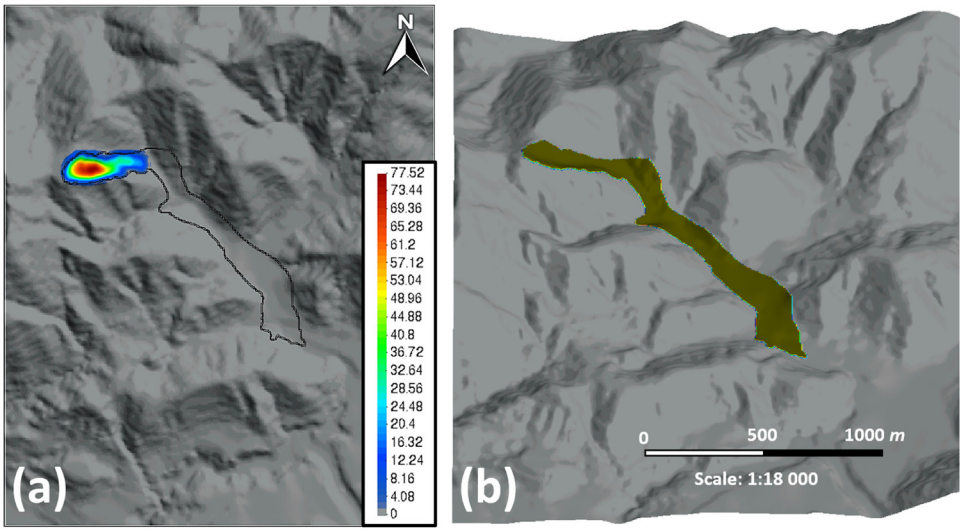


**Fig. 10.** The topography of the Acheron rock avalanche, including (a) the source area with the estimated release thicknesses in metres (contour lines) and (b) the observed impact area (green area). Data source: Mergili et al. [59]. (For interpretation of the references to colour in this figure legend, the reader is referred to the web version of this article.)

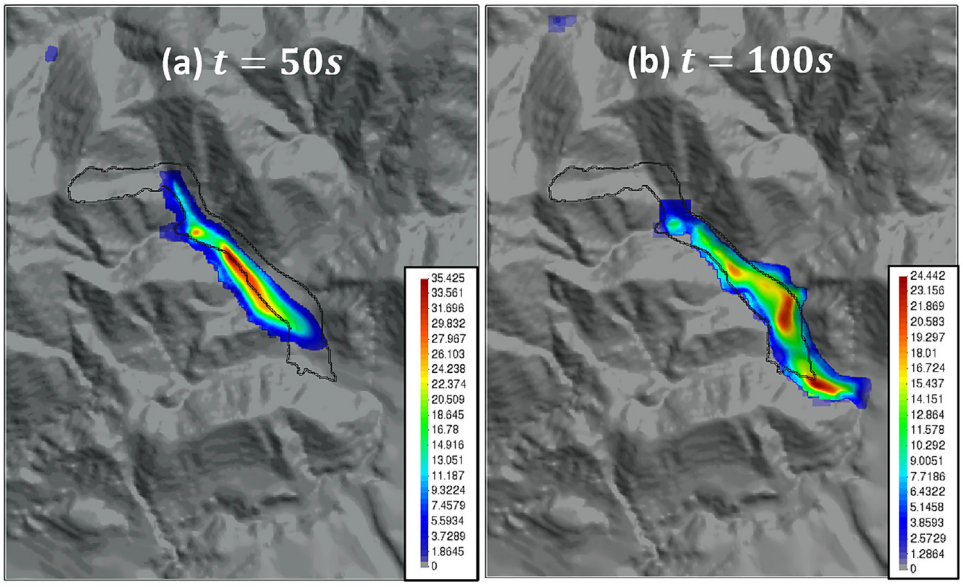


**Fig. 11.** The propagation of Acheron rock avalanche, consisting of low-permeability soil, accompanied by the numerical results of flow-depth in metres (contour lines) at times (a) 50 and (b) 100 s.

Consolidation time can be computed through Eq. (6) and is obtained as 200 s. As depicted in Fig. 11-b, the propagation time is 100 s, indicating that the pore-water pressure was preserved in the body of the flow during the propagation stage. Such these cases were represented by the third set of dam-break problems provided in the previous section. In Fig. 11-b, we can observe that the model overestimates the run-out distance of the debris avalanche. One important aspect of fast landslides with low-permeability soil is pore-water pressure generation due to strong coupling between solid and pore-fluid phases, which increases flows' velocity and run-out distance.

In the second scenario, we have modelled the flow by assuming that it consists of medium-permeability soil, choosing $V_T = 11 \times 10^{-4}$ m/s. This model was represented by the second set of dam-break problems provided in the previous section. In this case, the propagation and dissipation times are very close, obtained as 90 s. As shown in Fig. 12-b, the deposit shape obtained from the simulation does not match well with the observed deposit shape yet.

Regarding the last case with high permeability, the value of 0.01 m/s was chosen for the terminal velocity ($V_T$). Consolidation and propagation times are obtained as 10 s and 90 s, respectively, indicating that the pore-water pressure dissipates more rapidly, corresponding to high-permeability soil cases represented by the first set of dam-break problems provided in the previous section.

As shown in Fig. 13, the propagation material could well spread in all the observed impacted areas and cover almost the whole trimline. Therefore, the proposed model choosing high-permeability granular particles successfully reproduced the rock avalanche's propagation, deposition area shape and run-out distance. Therefore, using the proposed velocity-drag expressions, the presented model in this study can be applied to different case studies with different ranges of soil permeability, excess pore-water pressure, and relative velocity.

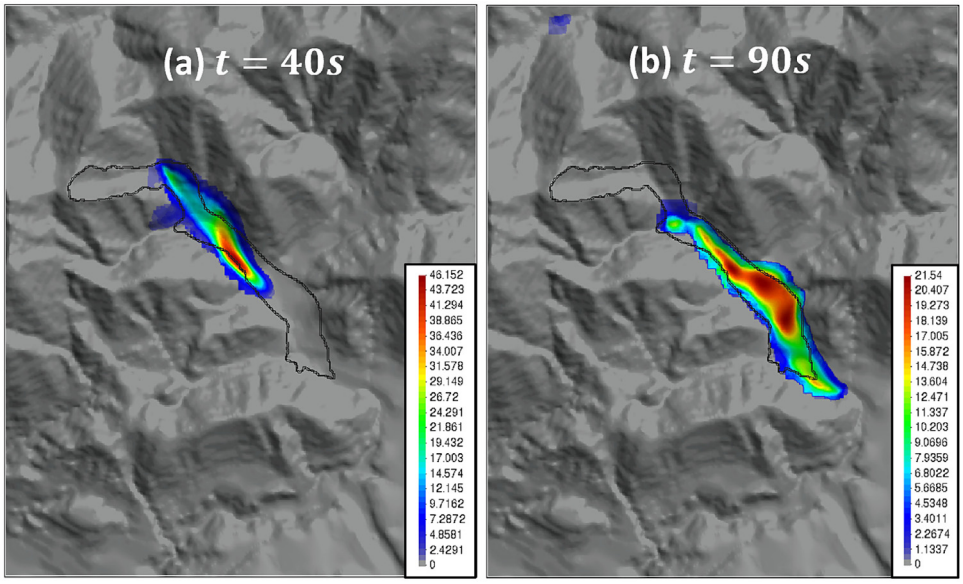


**Fig. 12.** The propagation of Acheron rock avalanche, consisting of medium-permeability soil, accompanied by the numerical results of flow-depth in metres (contour lines) at times (a) 40 and (b) 90 s.

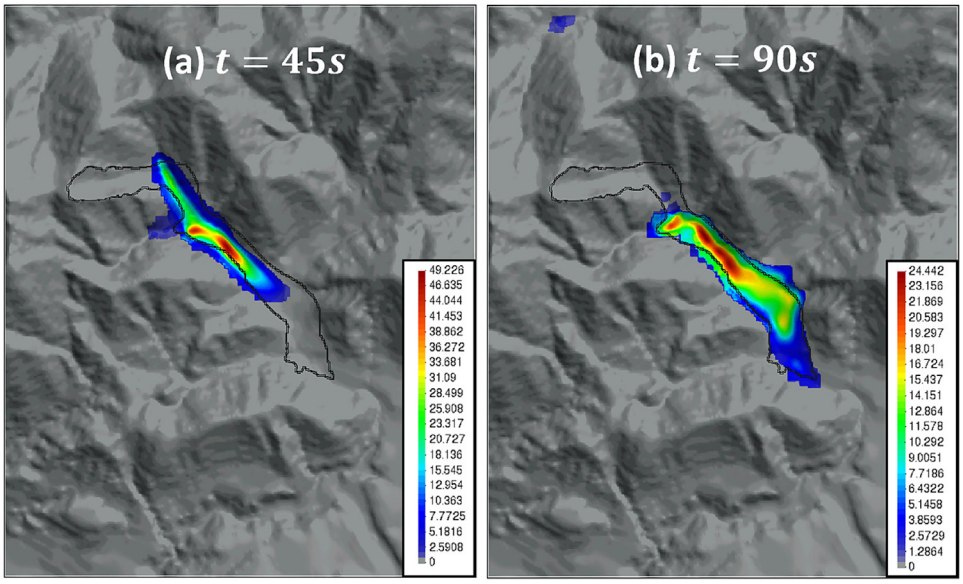


**Fig. 13.** The propagation of Acheron rock avalanche, consisting of high-permeability soil, accompanied by the numerical results of flow-depth in metres (contour lines) at times (a) 45 and (b) 90 s.

Fig. 14 shows the evolution of a front particle's positions and the highest relative pore-water pressure at different times. At the initial time, the relative pore-water pressure was taken as 1, indicating that the source materials were fully liquefied. As shown in Fig. 14, the dissipation rate of pore-water pressure is the lowest in the first scenario with low soil permeability and the highest in the last scenario with high soil permeability. The runout distances of the cases with low, medium, and high soil permeability are 3047 m, 2910 m, and 2730 m, respectively. The significant differences in these runout distances (minimum 137 m) indicate the importance of considering pore-water pressure in landslide propagation modelling.

## 4. Conclusion

This paper aims to present a generalized two-phase model, developed by the authors, capable of reproducing the complex dynamics behaviour of rapid landslides. The extended model is based on the mixture theory, in which balance equations of mass and linear momentum are established for each phase. The computational framework is based on mesh-free smoothed particle hydrodynamics (SPH). Although the two-phase model has been simplified to the depth-integrated type, the vertical structure of pore-water pressure is described through a consolidation equation implemented to the governing equations. To compute the vertical distribution of pore-water pressure, the consolidation equation is discretized with a 1D finite-difference mesh (SPH-FD model). The model employs a frictional rheological law capable of considering the evolution of basal pore-water pressure for the granular material, and the interstitial fluid is neglected due to its low value compared to the friction generated by the solid phase. A drag law is used to describe the interaction between grains and pore fluid in two-phase models and control the relative movement between the solid and fluid phases.

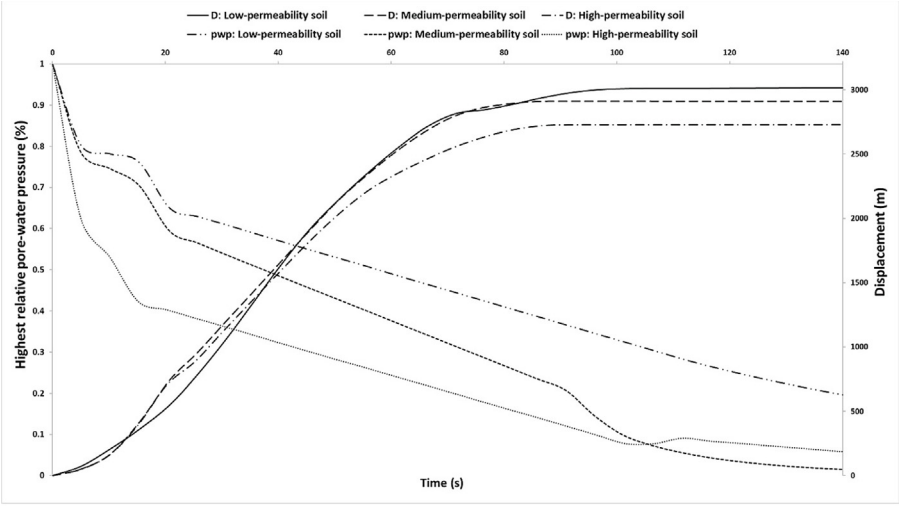


**Fig. 14.** Comparison of the front propagations and the relative pore-water pressure at each time step for the Acheron rock avalanche with different particle permeability (D: Displacement, pwp: pore-water pressure).

Thus, in this paper, a depth-integrated two-phase mathematical model has been extended to take into account the interaction between phases more precisely by considering three essential physical aspects, including soil permeability, porosity variation, and drag force. In the presented model, (i) the soil permeability is a key parameter to describe the time-space evolution of pore-water pressure, (ii) the porosity variation implemented in both equations of linear momentum and consolidation plays an important role, and (iii) the new drag–velocity formulation facilitates computing of velocities of both phases.

Three different dam-break problems have been simulated to study the dynamic behaviours of fast landslides with different soil permeability. In these exercises, the new velocity-drag formulation has also been tested. The flowing mass in the first dam-break problem represents granular flows such as rock avalanches where the permeability is high enough so that the consolidation time becomes much shorter than the time of propagation, and the material behaves as drained. The flow of the second dam-break problem represents a debris flow consisting of medium-permeability soil. In the third dam-break problem, a flow of slurries with a high water content was represented. In this case, the time of dissipation is much higher than the propagation time, and flow behaviour can be assumed to be undrained.

Besides, the extended model was capable of visualizing how the interstitial fluid phase and the solid skeleton move relative to each other. Different scenarios have been considered for dam-break problems, and the front propagation along time for each of the scenarios has been provided. The results indicated that run-out distance is strongly affected by the time-space evolution of the excess pore-water pressure, which depends on soil permeability and porosity variations.

The model was later used to simulate the Acheron rock avalanche that occurred in New Zealand in ancient history. The numerical results were compared to the field data, and it evidences that the model was capable of reproducing the run-out distance and deposition shape of the real case by using adequate back-calculated consolidation parameters. In particular, the following input variables have been tuned to minimize the differences between the numerical results and the available measures: basal friction angle, Voellmy turbulent coefficient, oedometric modulus, and porosity.

The results obtained with the extended model have been satisfactory and have shown us its potential. The simulations have revealed that this approach is suitable for rapid landslides in which solid particles and pore-fluid may have different velocities. The model is capable of including velocities of both solid and fluid phases and the interaction between them. Therefore, the developed two-phase propagation–consolidation model with a new solution for the interaction terms provides a good combination between accuracy and computational effort.

## List of symbols

| | | |
|---|---|---|
| $b_3$ | Gravity force ($b_3 = -\mathrm{g}$) | [m/s$^2$] |
| $\boldsymbol{b}$ | Vector of body forces | [m/s$^2$] |
| $C_d$ | Drag coefficient | [Ns/m$^4$] |
| $c_v$ | Consolidation coefficient | [m$^2$/s] |
| $E_m$ | Oedometric modulus | [N/m$^2$] |
| $e_R$ | Erosion coefficient | [m/s] |
| $h$ | Propagation height | [m] |
| $h_{\mathrm{sat}}$ | Saturated height | [m] |
| $k_v$ | Elastic volumetric stiffness | [N/m$^2$] |
| $k_w$ | Permeability tensor | [m$^4$/Ns] |
| $M$ | Fictitious volume | [m$^3$] |
| $m$ | Exponent for drag (1 for linear and 2 for quadratic) | [–] |
| $m_s$ | Mass of solid particle | [m$^3$] |
| $m_w$ | Mass of fluid particle | [m$^3$] |
| $\bar{n}$ | Averaged porosity | [–] |
| $n_L$ | Lower limit of porosity | [–] |
| $\bar{P}_s$ | A pressure term acting on solid phase | [m$^3$/s$^2$] |
| $\bar{P}_w$ | A pressure term acting on fluid phase | [m$^3$/s$^2$] |
| $\bar{\boldsymbol{R}}$ | Interaction force | [N/m$^3$] |
| $\bar{\boldsymbol{R}}^{(s)}$ | Force on the solid phase caused by the fluid phase | [N/m$^3$] |
| $\bar{\boldsymbol{R}}^{(w)}$ | Force on the fluid phase caused by the solid phase | [N/m$^3$] |
| $\bar{\boldsymbol{R}}_s$ | Force on a solid particle caused by a fluid particle | [N/m$^2$] |
| $\bar{\boldsymbol{R}}_w$ | Force on a fluid particle caused by a solid particle | [N/m$^2$] |
| $\mathrm{S_r}$ | Degree of saturation | [%] |
| $t_c$ | Consolidation time | [s] |
| $V_T$ | Terminal velocity | [m/s] |
| $\bar{\boldsymbol{v}}$ | Averaged velocity | [m/s] |
| $W$ | Smoothing kernel function | [–] |

| | | |
|---|---|---|
| $\Delta p_w$ | Excess pore-water pressure | [Pa] |
| $\Delta p_w^b$ | Excess pore-water pressure at the basal surface | [Pa] |
| $\nu$ | Poisson's ratio | [–] |
| $\xi$ | Turbulence coefficient | [m/s$^2$] |
| $\rho$ | Density | [kg/m$^3$] |
| $\rho_d{}'$ | Effective density $\left(\bar{\rho}' = \rho - \rho_w\right)$ | [kg/m$^3$] |
| $\boldsymbol{\tau}_B$ | Basal shear stress | [N/m$^2$] |
| $\phi_B$ | Basal friction angle | [°] |

## Declaration of competing interest

The authors declare that they have no known competing financial interests or personal relationships that could have appeared to influence the work reported in this paper.

## Acknowledgements

The authors gratefully acknowledge the economic support provided by the Spanish Ministry MINECO under project P-LAND (PID2019-105630GB-I00).

## References

[1] R.A. Bagnold, Experiments on a gravity-free dispersion of large solid spheres in a Newtonian fluid under shear, Proc. R. Soc. Lond. Ser. A Math. Phys. Eng. Sci. 225 (1160) (1954) 49–63, http://dx.doi.org/10.1098/rspa.1954.0186, URL http://www.royalsocietypublishing.org/doi/10.1098/rspa.1954.0186.

[2] S.B. Savage, K. Hutter, The motion of a finite mass of granular material down a rough incline, J. Fluid Mech. 199 (1989) 177–215.

[3] S.B. Savage, K. Hutter, The dynamics of avalanches of granular materials from initiation to runout. Part I: Analysis, Acta Mech. 86 (1–4) (1991) 201–223, http://dx.doi.org/10.1007/BF01175958, URL http://link.springer.com/10.1007/BF01175958.

[4] R.M. Iverson, The physics of debris flows, Rev. Geophys. 35 (3) (1997) 245–296, http://dx.doi.org/10.1029/97RG00426, URL http://doi.wiley.com/10.1029/97RG00426.

[5] R.M. Iverson, R.P. Denlinger, Flow of variably fluidized granular masses across three-dimensional terrain: 1. Coulomb mixture theory, J. Geophys. Res. Solid Earth 106 (B1) (2001) 537–552, http://dx.doi.org/10.1029/2000JB900329, URL http://doi.wiley.com/10.1029/2000JB900329.

[6] M. Pastor, M. Quecedo, J.A. Merodo, M.I. Herrores, E. Gonzalez, P. Mira, Modelling tailings dams and mine waste dumps failures, Géotechnique 52 (8) (2002) 579–591, http://dx.doi.org/10.1680/geot.2002.52.8.579, URL http://www.icevirtuallibrary.com/doi/10.1680/geot.2002.52.8.579.

[7] M. Pastor, B. Haddad, G. Sorbino, S. Cuomo, V. Drempetic, A depth-integrated, coupled SPH model for flow-like landslides and related phenomena, Int. J. Numer. Anal. Methods Geomech. 33 (2) (2009) 143–172, http://dx.doi.org/10.1002/nag.705, URL http://doi.wiley.com/10.1002/nag.705.

[8] E.B. Pitman, L. Le, A two-fluid model for avalanche and debris flows, Philos. Trans. R. Soc. Lond. Ser. A Math. Phys. Eng. Sci. 363 (1832) (2005) 1573–1601, http://dx.doi.org/10.1098/rsta.2005.1596, URL http://www.royalsocietypublishing.org/doi/10.1098/rsta.2005.1596.

[9] S.P. Pudasaini, A general two-phase debris flow model, J. Geophys. Res. Earth Surf. 117 (F3) (2012) F03010, http://dx.doi.org/10.1029/2011JF002186, URL http://doi.wiley.com/10.1029/2011JF002186.

[10] M. Pastor, A. Yague, M.M. Stickle, D. Manzanal, P. Mira, A two-phase SPH model for debris flow propagation, Int. J. Numer. Anal. Methods Geomech. 42 (3) (2018) 418–448, http://dx.doi.org/10.1002/nag.2748, URL http://doi.wiley.com/10.1002/nag.2748.

[11] S.A.M. Tayebi, S.M. Tayyebi, M. Pastor, Depth-integrated two-phase modeling of two real cases: A comparison between r.avaflow and GeoFlow-SPH codes, Appl. Sci. 11 (12) (2021) 5751, http://dx.doi.org/10.3390/app11125751, URL https://www.mdpi.com/2076-3417/11/12/5751.

[12] H.H. Bui, K. Sako, R. Fukagawa, Numerical simulation of soil–water interaction using smoothed particle hydrodynamics (SPH) method, J. Terramechanics 44 (5) (2007) 339–346, http://dx.doi.org/10.1016/j.jterra.2007.10.003, URL https://linkinghub.elsevier.com/retrieve/pii/S0022489807000559.

[13] M. Pastor, S.M. Tayyebi, M.M. Stickle, A. Yagüe, M. Molinos, P. Navas, D. Manzanal, A depth integrated, coupled, two-phase model for debris flow propagation, Acta Geotech. (2021) 1–25, http://dx.doi.org/10.1007/s11440-020-01114-4, URL http://link.springer.com/10.1007/s11440-020-01114-4.

[14] O.C. Zienkiewicz, T. Shiomi, Dynamic behaviour of saturated porous media; The generalized Biot formulation and its numerical solution, Int. J. Numer. Anal. Methods Geomech. 8 (1) (1984) 71–96, http://dx.doi.org/10.1002/nag.1610080106, URL http://doi.wiley.com/10.1002/nag.1610080106.

[15] S.M. Tayyebi, M. Pastor, A.L. Yifru, V.K.S. Thakur, M.M. Stickle, Two-phase SPH–FD depth-integrated model for debris flows: Application to basal grid brakes, Géotechnique (2021) 1–16, http://dx.doi.org/10.1680/jgeot.21.00080, URL https://www.icevirtuallibrary.com/doi/10.1680/jgeot.21.00080.

[16] S.M. Tayyebi, M. Pastor, M. Stickle, Two-phase SPH numerical study of pore-water pressure effect on debris flows mobility: Yu Tung debris flow, Comput. Geotech. 132 (2021) 103973, http://dx.doi.org/10.1016/j.compgeo.2020.103973, URL https://linkinghub.elsevier.com/retrieve/pii/S0266352X2030536X.

[17] J.N. Hutchinson, A sliding–consolidation model for flow slides, Can. Geotech. J. 23 (2) (1986) 115–126, http://dx.doi.org/10.1139/t86-021, URL http://www.nrcresearchpress.com/doi/10.1139/t86-021.

[18] L.B. Lucy, A numerical approach to the testing of the fission hypothesis, Astron. J. 82 (1977) 1013–1024, http://dx.doi.org/10.1086/112164.

[19] R.A. Gingold, J.J. Monaghan, Smoothed particle hydrodynamics - Theory and application to non-spherical stars, Mon. Not. R. Astron. Soc. 181 (1977) 375–389, http://dx.doi.org/10.1093/mnras/181.3.375.

[20] S. McDougall, A New Continuum Dynamic Model for the Analysis of Extremely Rapid Landslide Motion Across Complex 3D Terrain (Ph.D. thesis), University of British Columbia, 2006, p. 253.

[21] E. Yang, H.H. Bui, H. De Sterck, G.D. Nguyen, A. Bouazza, A scalable parallel computing SPH framework for predictions of geophysical granular flows, Comput. Geotech. 121 (2020) 103474, http://dx.doi.org/10.1016/j.compgeo.2020.103474, URL https://linkinghub.elsevier.com/retrieve/pii/S0266352X20300379.

[22] M. Pastor, M. Quecedo, E. Gonzalez, M.I. Herreros, J.A. Merodo, P. Mira, Modelling of landslides: (II) propagation, in: F. Darve, I. Vardoulakis (Eds.), Degrad. Instab. Geomaterials, Springer Vienna, Vienna, 2004, pp. 319–367, http://dx.doi.org/10.1007/978-3-7091-2768-1_11, URL http://link.springer.com/10.1007/978-3-7091-2768-1{_}11.

[23] L. Cascini, S. Cuomo, M. Pastor, G. Sorbino, L. Piciullo, SPH run-out modelling of channelised landslides of the flow type, Geomorphology 214 (2014) 502–513, http://dx.doi.org/10.1016/j.geomorph.2014.02.031, URL https://linkinghub.elsevier.com/retrieve/pii/S0169555X1400124X.

[24] L. Cascini, S. Cuomo, M. Pastor, I. Rendina, SPH-FDM propagation and pore water pressure modelling for debris flows in flume tests, Eng. Geol. 213 (2016) 74–83, http://dx.doi.org/10.1016/j.enggeo.2016.08.007, URL https://linkinghub.elsevier.com/retrieve/pii/S0013795216302472.

[25] S. Cuomo, M. Pastor, L. Cascini, G.C. Castorino, Interplay of rheology and entrainment in debris avalanches: A numerical study, Can. Geotech. J. 51 (11) (2014) 1318–1330, http://dx.doi.org/10.1139/cgj-2013-0387, URL http://www.nrcresearchpress.com/doi/10.1139/cgj-2013-0387.

[26] S. Cuomo, M. Pastor, V. Capobianco, L. Cascini, Modelling the space–time evolution of bed entrainment for flow-like landslides, Eng. Geol. 212 (2016) 10–20, http://dx.doi.org/10.1016/j.enggeo.2016.07.011, URL https://linkinghub.elsevier.com/retrieve/pii/S0013795216302277.

[27] M. Pastor, T. Blanc, M.J. Pastor, A depth-integrated viscoplastic model for dilatant saturated cohesive-frictional fluidized mixtures: Application to fast catastrophic landslides, J. Non-Newton. Fluid Mech. 158 (1–3) (2009) 142–153, http://dx.doi.org/10.1016/j.jnnfm.2008.07.014, URL https://linkinghub.elsevier.com/retrieve/pii/S0377025708001559.

[28] S. McDougall, O. Hungr, A model for the analysis of rapid landslide motion across three-dimensional terrain, Can. Geotech. J. 41 (6) (2004) 1084–1097, http://dx.doi.org/10.1139/t04-052, URL http://www.nrcresearchpress.com/doi/10.1139/t04-052.

[29] M. Rodriguez-Paz, J. Bonet, A corrected smooth particle hydrodynamics formulation of the shallow-water equations, Comput. Struct. 83 (17–18) (2005) 1396–1410, http://dx.doi.org/10.1016/j.compstruc.2004.11.025, URL https://linkinghub.elsevier.com/retrieve/pii/S0045794905000714.

[30] G.R. Goodwin, C.E. Choi, A depth-averaged SPH study on spreading mechanisms of geophysical flows in debris basins: Implications for terminal barrier design requirements, Comput. Geotech. 141 (2022) 104503, http://dx.doi.org/10.1016/j.compgeo.2021.104503, URL https://linkinghub.elsevier.com/retrieve/pii/S0266352X21004845.

[31] S. Li, W.K. Liu, Meshfree Particle Methods, first ed., Springer-Verlag, Berlin Heidelberg, 2004, http://dx.doi.org/10.1007/978-3-540-71471-2.

[32] G.R. Liu, M.B. Liu, Smoothed Particle Hydrodynamics: A Meshfree Particle Method, World Scientific, 2003, p. 472, http://dx.doi.org/10.1142/5340, URL http://www.worldscientific.com/worldscibooks/10.1142/5340.

[33] H. Cheng, Y. Huang, W. Zhang, Q. Xu, Physical process-based runout modeling and hazard assessment of catastrophic debris flow using SPH incorporated with ArcGIS: A case study of the Hongchun gully, CATENA 212 (2022) 106052, http://dx.doi.org/10.1016/j.catena.2022.106052, URL https://linkinghub.elsevier.com/retrieve/pii/S0341816222000388.

[34] Y. Wu, A. Tian, H. Lan, Comparisons of dynamic landslide models on GIS platforms, Appl. Sci. 12 (6) (2022) 3093, http://dx.doi.org/10.3390/app12063093, URL https://www.mdpi.com/2076-3417/12/6/3093.

[35] S. Manenti, A. Amicarelli, S. Todeschini, WCSPH with limiting viscosity for modeling landslide hazard at the slopes of artificial reservoir, Water 10 (4) (2018) 515, http://dx.doi.org/10.3390/w10040515, URL http://www.mdpi.com/2073-4441/10/4/515.

[36] S. Manenti, A. Amicarelli, N. Palazzolo, M. Bordoni, E. Creaco, C. Meisina, Post-failure dynamics of rainfall-induced landslide in Oltrepò Pavese, Water 12 (9) (2020) 2555, http://dx.doi.org/10.3390/w12092555, URL https://www.mdpi.com/2073-4441/12/9/2555.

[37] M. Pastor, T. Blanc, B. Haddad, V. Drempetic, M.S. Morles, P. Dutto, M.M. Stickle, P. Mira, J.A. Merodo, Depth averaged models for fast landslide propagation: Mathematical, rheological and numerical aspects, Arch. Comput. Methods Eng. 22 (1) (2015) 67–104, http://dx.doi.org/10.1007/s11831-014-9110-3, URL http://link.springer.com/10.1007/s11831-014-9110-3.

[38] C. Hirsch, Numerical Computation of Internal &Amp; External Flows: Fundamentals of Numerical Discretization, John Wiley & Sons, Inc., New York, NY, USA, 1988,

[39] A. Voellmy, Uber Die Zerstorungskraft Von Lawinen, Schweizerische Bauzeitung, 1955.

[40] T.B. Anderson, R. Jackson, Fluid mechanical description of fluidized beds. Equations of motion, Ind. Eng. Chem. Fundam. 6 (4) (1967) 527–539, http://dx.doi.org/10.1021/i160024a007, https://pubs.acs.org/doi/abs/10.1021/i160024a007.

[41] J. Kozeny, Ueber kapillare leitung des wassers im boden, Sitzungsber Akad. Wiss., Wien 136 (2a) (1927) 271–306.

[42] P.C. Carman, Fluid flow through granular beds, Trans. Inst. Chem. Eng. (15) (1937) 150–166.

[43] P.C. Carman, Flow of Gases Through Porous Media, Butterworths, London, 1956.

[44] B. Haddad, M. Pastor, D. Palacios, E. Muñoz-Salinas, A SPH depth integrated model for Popocatépetl 2001 lahar (Mexico): Sensitivity analysis and runout simulation, Eng. Geol. 114 (3–4) (2010) 312–329, http://dx.doi.org/10.1016/j.enggeo.2010.05.009, URL https://linkinghub.elsevier.com/retrieve/pii/S0013795210000839.

[45] M. Pastor, T. Blanc, B. Haddad, S. Petrone, M. Sanchez Morles, V. Drempetic, D. Issler, G.B. Crosta, L. Cascini, G. Sorbino, S. Cuomo, Application of a SPH depth-integrated model to landslide run-out analysis, Landslides 11 (5) (2014) 793–812, http://dx.doi.org/10.1007/s10346-014-0484-y, URL http://link.springer.com/10.1007/s10346-014-0484-y.

[46] J. Krušić, B. Abolmasov, M. Marjanović, M.J. Pastor, S.M. Tayyebi, Numerical modeling of selanac debris flow propagation using SPH code, in: 13th Int. Symp. Landslides, 2021, URL https://www.issmge.org/publications/publication/numerical-modeling-of-selanac-debris-flow-propagation-using-sph-code.

[47] C. Lin, M. Pastor, A. Yague, S.M. Tayyebi, M.M. Stickle, D. Manzanal, T. Li, X. Liu, A depth-integrated SPH model for debris floods: Application to Lo Wai (Hong Kong) debris flood of August 2005, Géotechnique (2019) 1–21, http://dx.doi.org/10.1680/jgeot.17.P.267, https://www.icevirtuallibrary.com/doi/10.1680/jgeot.17.p.267.

[48] O. Hungr, S. McDougall, M. Bovis, Entrainment of material by debris flows, in: Debris-Flow Hazards Relat. Phenom, Springer Berlin Heidelberg, Berlin, Heidelberg, 2005, pp. 135–158, http://dx.doi.org/10.1007/3-540-27129-5_7, URL http://link.springer.com/10.1007/3-540-27129-5{_}7.

[49] S. Egashira, Mechanism of sediment erosion and deposition of debris flow, Jpn. Soc. Eros. Control Eng. 46 (No.1 (186)) (1993) 45–49.

[50] M. Pirulli, M. Pastor, Numerical study on the entrainment of bed material into rapid landslides, Géotechnique 62 (11) (2012) 959–972, http://dx.doi.org/10.1680/geot.10.P.074, URL http://www.icevirtuallibrary.com/doi/10.1680/geot.10.P.074.

[51] M. Pastor, S.M. Tayyebi, M.M. Stickle, M. Molinos, A. Yague, D. Manzanal, P. Navas, An arbitrary Lagrangian Eulerian (ALE) finite difference (FD)-SPH depth integrated model for pore pressure evolution on landslides over erodible terrains, Int. J. Numer. Anal. Methods Geomech. 46 (6) (2022) 1127–1153, http://dx.doi.org/10.1002/nag.3339, URL https://onlinelibrary.wiley.com/doi/10.1002/nag.3339.

[52] W. Benz, Smooth particle hydrodynamics: A review, in: J. Buchler (Ed.), Numer. Model. Nonlinear Stellar Pulsations, Springer Netherlands, Dordrecht, 1990, pp. 269–288, http://dx.doi.org/10.1007/978-94-009-0519-1_16, URL http://link.springer.com/10.1007/978-94-009-0519-1{_}16.

[53] J.J. Monaghan, R.A. Gingold, Shock simulation by the particle method SPH, J. Comput. Phys. 52 (2) (1983) 374–389, http://dx.doi.org/10.1016/0021-9991(83)90036-0, URL https://linkinghub.elsevier.com/retrieve/pii/0021999183900360.

[54] A. Amicarelli, B. Kocak, S. Sibilla, J. Grabe, A 3D smoothed particle hydrodynamics model for erosional dam-break floods, Int. J. Comput. Fluid Dyn. 31 (10) (2017) 413–434, http://dx.doi.org/10.1080/10618562.2017.1422731, URL https://www.tandfonline.com/doi/full/10.1080/10618562.2017.1422731.

[55] F.E. Toro, Shock-Capturing Methods for Free-Surface Shallow Flows, Wiley, 2001, p. 328.

[56] B.D. Rogers, R.A. Dalrymple, P.K. Stansby, Simulation of caisson breakwater movement using 2-D SPH, J. Hydraul. Res. 48 (sup1) (2010) 135–141, http://dx.doi.org/10.1080/00221686.2010.9641254, URL https://www.tandfonline.com/doi/full/10.1080/00221686.2010.9641254.

[57] G.M. Smith, T.R. Davies, M.J. McSaveney, D.H. Bell, The acheron rock avalanche, Canterbury, New Zealand—Morphology and dynamics, Landslides 3 (1) (2006) 62–72, http://dx.doi.org/10.1007/s10346-005-0012-1, URL http://link.springer.com/10.1007/s10346-005-0012-1.

[58] G.M. Smith, D.H. Bell, T.R.H. Davies, The acheron rock avalanche deposit, Canterbury, New Zealand: Age and implications for dating landslides, New Zealand J. Geol. Geophys. 55 (4) (2012) 375–391, http://dx.doi.org/10.1080/00288306.2012.733947, URL http://www.tandfonline.com/doi/abs/10.1080/00288306.2012.733947.

[59] M. Mergili, J. Fischer, J. Krenn, S.P. Pudasaini, R.avaflow v1, an advanced open-source computational framework for the propagation and interaction of two-phase mass flows, Geosci. Model Dev. 10 (2) (2017) 553–569, http://dx.doi.org/10.5194/gmd-10-553-2017, URL https://gmd.copernicus.org/articles/10/553/2017/.